# Automated In Vitro Wound Healing Assay

Jillian Cwycyshyn[1, 2], Cooper Stansbury[2, 3], Walter Meixner[2], James B. Hoying[4], Lindsey A. Muir[2], and Indika Rajapakse[1, 2, 5]

[1]Department of Biomedical Engineering, University of Michigan, Ann Arbor, MI 48109 USA
[2]Department of Computational Medicine and Bioinformatics, University of Michigan, Ann Arbor, MI 48109 USA
[3]The Michigan Institute for Computational Discovery and Engineering, University of Michigan, Ann Arbor, MI 48109 USA
[4]Advanced Solutions Life Sciences, Manchester, NH 03101 USA
[5]Department of Mathematics, University of Michigan, Ann Arbor, MI 48109 USA

November 2023

## Abstract

Wound healing is crucial for the restoration of the epidermal barrier in response to injury. This dynamic process requires an intricate orchestration of cellular migration and proliferation. Our understanding of the intra-cellular signalling mechanisms that initialize, cease, and balance migration and proliferation during wound healing remains incomplete. Wound healing assays are a frequently used approach to examine this complex relationship in vitro. However, existing assays suffer from limited reproducibility, low throughput, and inflexibility in experimental design. We have developed the Automated Wound Healing (AWH) assay, a high-throughput robotics-assisted technique for reproducible wound creation and automated time-lapse image analysis. Wounds are designed as Computer-aided design (CAD) models and recreated in confluent cell layers by the BioAssemblyBot (BAB) 3D-bioprinting platform. The dynamics of migration and proliferation in individual cells are evaluated over the course of wound closure using live-cell fluorescence microscopy and our image processing pipeline. The AWH assay outperforms the standard scratch assay with enhanced consistency in wound geometry. Our ability to create diverse wound shapes in any multi-well plate with the BAB not only allows for multiple experimental conditions to be analyzed in parallel but also offers versatility in the design of wound healing experiments. Our method emerges as a valuable tool for the automated completion and analysis of high-throughput, reproducible, and adaptable in vitro wound healing assays.

## Background

The wound healing process requires precise temporal and spatial coordination between different cell types and signaling mechanisms to effectively restore epidermal function [1–3]. Broadly, wound healing consists of four overlapping subprocesses: hemostasis, inflammation,

reepithelialization, and tissue remodeling [1, 4] (Figure 1A). Disruptions to this system can lead to excessive scar formation or the development of diabetic ulcers, keloids, and other chronic non-healing wounds [4–6]. The repercussions of impaired wound healing also extend beyond chronic wounds to severe skin injuries where precise cellular responses are paramount for optimal tissue regeneration. In cases of deep skin trauma and thermal burn wounds, the intricacies of the wound healing cascade become even more crucial.

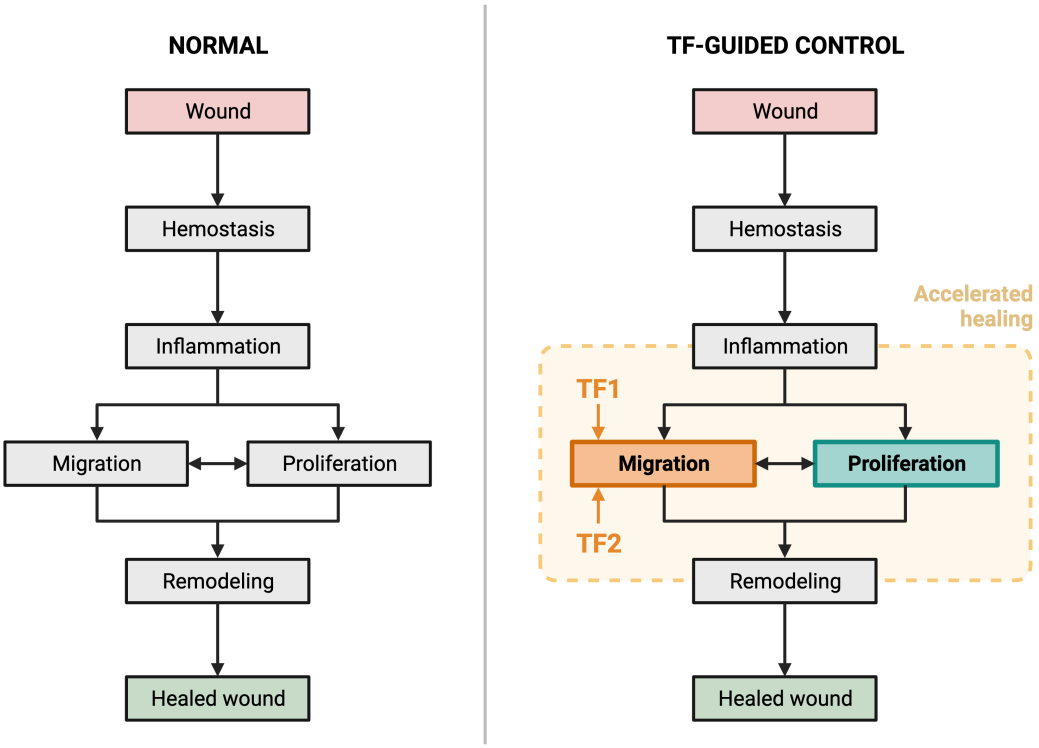


Figure 1: **The wound healing process.** Hemostasis, inflammation, reepithelialization, and tissue remodeling are overlapping processes that take place throughout the course of wound healing. During reepithelialization, cellular migration and proliferation are delicately balanced to restore tissue function. We aim to implement a transcription factor-guided approach that targets cell migration to accelerate the wound healing process. Figure created with BioRender.com

Cellular reprogramming offers exciting possibilities for the regeneration of diverse biological tissues, including chronic non-healing wounds and severe burns. We aim to implement a data-guided direct reprogramming approach to accelerate the wound healing process [7]. We envision that the delivery of targeted transcription factors (TFs) to wounded cells can expedite migration and proliferation during the healing process, accelerating the restoration of a healthy cellular state (Figure 1B). Evaluating reprogramming efficacy requires a reproducible in vitro wound healing model. Traditional methods, like the scratch assay, are simple and cost-effective but lack reproducibility, throughput, and experimental flexibility [8]. Several technologies have been developed to automate the creation of scratch wounds in 96-well plates [9, 10]. However, these methods create uniform scratches in all wells simultaneously which limits versatility in testing multiple experimental conditions or diverse

wounds types (e.g. incisions, lacerations, punctures).

The integration of robotic systems in biological research has revolutionized our ability to conduct complex assays [11]. Within the context of wound healing, robotics-assisted automation provides a compelling opportunity to develop a reproducible, high-throughput, and adaptable wound healing assay that can be used for evaluating reprogramming strategies geared towards accelerating the healing process. Herein, we present the automated wound healing assay (AWH)—a robotically-controlled approach to consistently create monolayer wounds and analyze cellular migration and proliferation across those wounds throughout the course of wound closure. Our method enables researchers to implement a wound healing assay in any-sized cell culture well plate, with the novel ability to generate customized wounds using an intelligent six-axis robotic arm, termed the BioAssemblyBot (BAB). The BAB is designed for 3D bioprinting and the completion of complex assays. Using the BAB's built-in printing workflow and 3D modelling software, wounds are designed as 3D shapes flattened onto the culture surface of a pre-calibrated well plate. CAD wound models are then sent to the BAB as a "3D print", where the AWH is executed and the designed wounds are created in confluent cell layers. Wound closure is subsequently monitored over time via live-cell fluorescence microscopy, enabling both the migratory and proliferative activities of individual cells to be tracked throughout the course of healing.

# Results

## Design and development of the automated wound healing assay

Wounding in the AWH assay is emulated through the creation of a cell-free region in a confluent cell layer. Cells within the programmed wound shapes are mechanically removed with a high-resolution dispensing tip on the end of the BAB Printing Tool (Figure 2A). The speed and pressure applied during wounding is highly precise, resulting in consistent wound dimensions and a reduced risk of damaging the cells or culture surface.

The AWH assay is implemented in three steps: 1) plate calibration, 2) wound design, and 3) execution (Figure 2B-D). Based on the needs of a given experiment, a desired well plate is calibrated with the BAB to program the x, y, and z coordinates for the center of all wells relative to the print stage. Likewise, the offset between the print stage and the plate surface is quantified to automatically update the calibrated z coordinates based on the specific plate and printing tip used (Figure 2B). Wounds are designed as CAD models in the Tissue Structure and Information Modeling (TSIM) software. TSIM provides the option to select a pre-calibrated well plate template for designing and printing the wounds. Here, wound shape, size, and placement within the wells are customized for the specific requirements of a given experiment (Figure 2C). The 3D wound models are then sent to the BAB, where the user selects their calibrated plate as the container for printing. The AWH assay is executed by pressing "GO" in the BAB user interface (Figure 2D).

## Live-cell fluorescent microscopy enables monitoring of migration and proliferation in individually tracked cells

A crucial component of any wound healing assay is capturing high-quality time-lapse images while the cells proliferate and migrate to fill the wound. The BAB is capable of interfacing with other laboratory equipment, such as live-cell imaging systems, through the BioApps

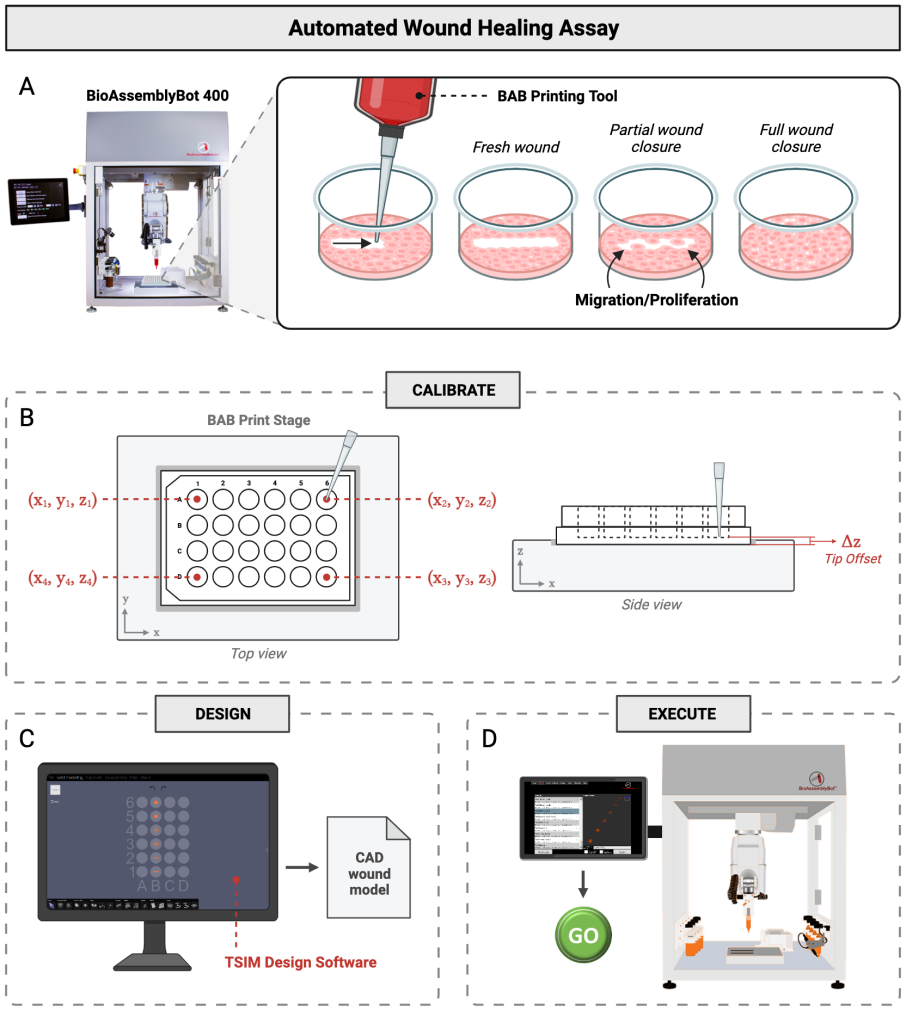


Figure 2: **Overview of the automated wound healing assay.** The BioAssembly Platform, including the BioAssemblyBot 400 (BAB) and the TSIM design software, is used for the automation of wound healing assays to increase reproducibility, scalability, and controllability of wound healing experiments. **(A)** The BAB simulates wound healing in any multi-well plate (6- to 96-well) by mechanically removing user-defined regions from confluent cell monolayers with the BAB Printing Tool to generate "wounds". Migration and proliferation are assessed in wound-adjacent cells over the duration of wound closure. **(B)** To perform the automated wound healing assay, the desired well plate must first be calibrated with the BAB. This involves determining the spatial coordinates of each corner of the plate and measuring the tip-to-stage offset between the end of the BAB Printing Tool (tip) and the bottom surface of the wells. **(C)** 3D models of the wounds are designed and created using the TSIM software. The resultant CAD files are then exported to the BAB, where **(D)** the assay is executed by pressing "GO" in the BAB HMI. Figure created with BioRender.com

Maker workflow management software. BioApps Maker enables researchers to stitch together various steps of an experiment to automate entire workflows. Utilizing this feature in the AWH assay, the BAB transfers the "wounded" well plate to the Zeiss Celldiscoverer 7

(CD7) live-cell fluorescent microscope where image acquisition is initiated. Here, time-lapse images of the cells are captured at least every 30 minutes until the wound is fully closed. Acquired images are ran through our image processing pipeline which detects and tracks individual cell nuclei, both proximal and distal to the wound (Figure 3A). Thus, cell divisions and migration patterns are quantified at the single-cell level over time. The dynamics of collective cell migration can also be observed throughout the course of wound healing (Figure 3B).

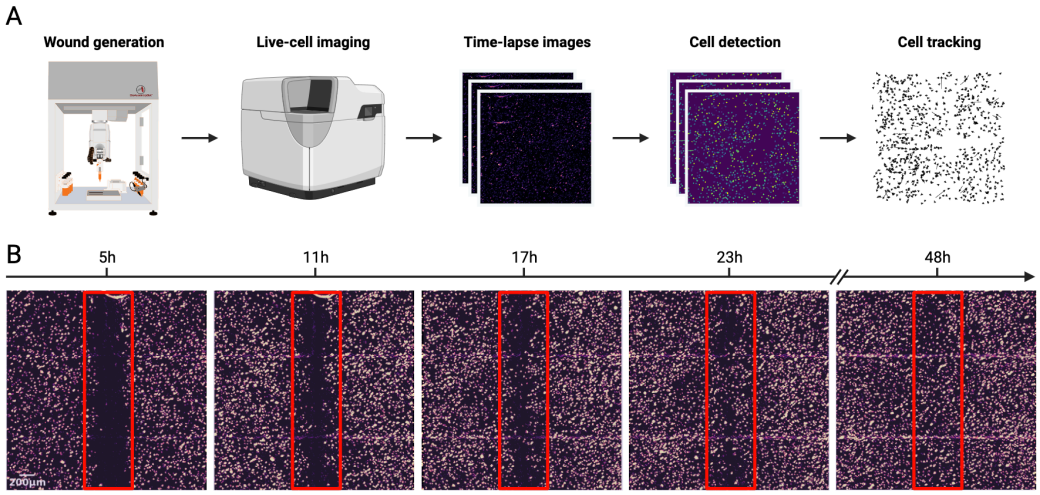


Figure 3: **Workflow for the automated wound healing assay and time-lapse image analysis. (A)** The AWH is performed as described in Figure 2. By use of the BioApps Maker workflow automater, the BAB is programmed to transfer the well plate to the Zeiss Celldiscoverer7 (CD7) and begin image acquisition. Images are taken at 20-30 minute intervals over the course of wound closure. Individual cells are detected in each image, and the migration trajectory for each cell is tracked over time. **(B)** Representative images of wound closure over time for a simple scratch wound. Scale bar = 200 $\mu$m. Figure created with BioRender.com

## The automated wound healing assay produces consistent wound dimensions with control over wound shape

To compare the performance of the AWH assay against the standard scratch assay, simple scratches were applied to human neonatal fibroblasts by the BAB and manually. Images of each well were taken at 5x magnification, and manual- and BAB-generated scratch geometries were evaluated for consistency in the wound edge. In short, the horizontal positions (x-axis coordinate) of contour points along the wound edge were identified for each image. The image-wide average x position was then subtracted from each of these values to provide the distance from the center of the wound to the wound edge. The AWH assay produces wounds with increased consistency in wound geometry across all wells compared to wounds that were created manually (Figure 4A). We observed lower variability in the wound edge for wounds generated by the BAB (14.948 $\pm$ 14.785) than for wounds generated manually (20.5601 $\pm$ 19.394) (Table 1). These results highlight the precision in machine-generated wounds.

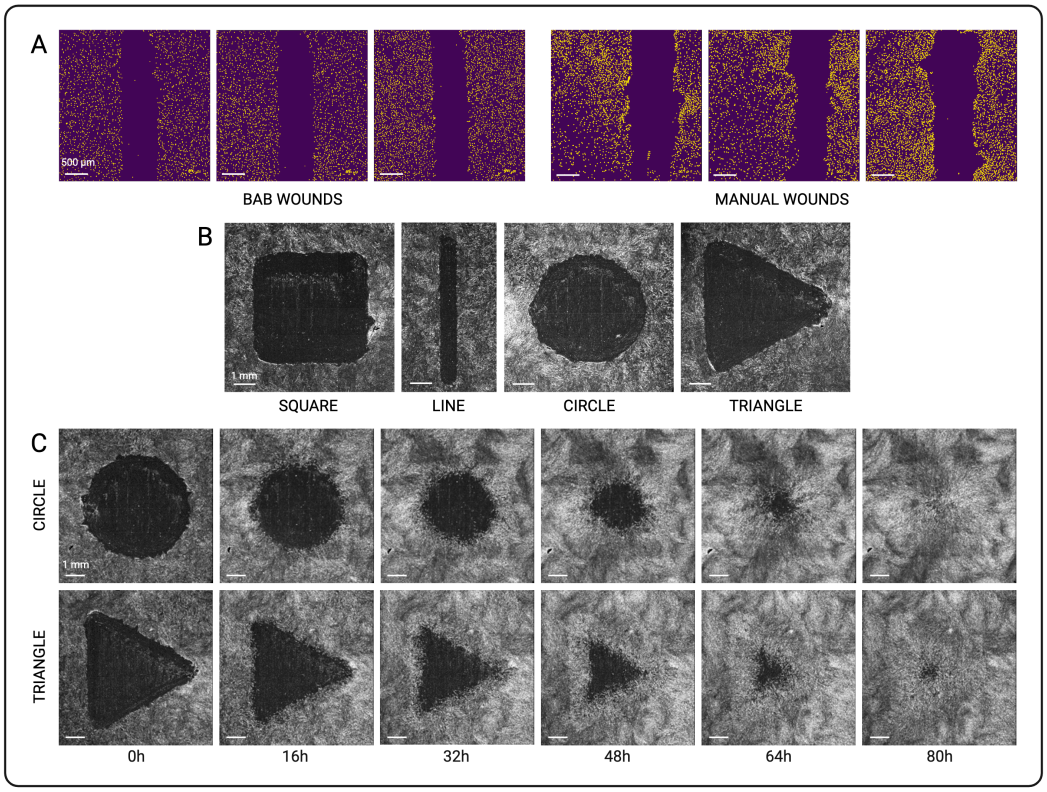


Figure 4: **Preliminary results show increased consistency and controllability over wound dimensions compared to the standard scratch assay. (A)** Representative images of simple scratches made by the BAB (Left) and by hand (Right). BAB-generated wounds exhibit more consistency in the wound edge compared to manually generated wounds. Scale bar = 500 $\mu$m. **(B)** The BAB can create multiple different wound shapes, including a square, line, circle, and triangle. Scale bar = 1 mm. **(C)** Image montage of wound closure over time for the circle and triangle shapes. Scale bar = 1 mm. Figure created with BioRender.com

| **Method** | **Mean** | **SD** |
|---|---|---|
| AWH assay | 14.948 | 14.785 |
| Manual scratch | 20.5601 | 19.394 |

Table 1: **Wound Edge Variability (N=3).** Values are based off of the average distance from the center of the wound to contour points along the wound edge.

To demonstrate the BAB's ability to create differently shaped wounds, four distinct wounds were generated in fibroblast monolayers (Figure 4B). Images of each well were taken at 5x magnification every 20 minutes over an 88-hour period to monitor the rate of wound closure for each shape. When designing AWH experiments, the area of the wound largely determines the time it will take for the wound to fully close. Wounds with larger areas, such as the circle, square, or triangle, take the longest time to close, while wounds with smaller

areas, such as the line, exhibit a noticeably shorter closure time (Table 2). Thus, in a given experiment, wound sizes need to be carefully designed in order to achieve full wound closure during image acquisition. Representative images of different wound shapes closing over time are depicted in Figure 4C.

| **Wound** | **Area ($mm^2$) ± SD** | **Closure time** | **% Closure ($t = 88$ hr)** |
|---|---|---|---|
| Triangle | 21.579 ± 0.366 | >88 hr | 98.79% |
| Square | 17.574 ± 0.862 | >88 hr | 99.94% |
| Circle | 17.148 ± 1.0681 | >88 hr | 99.64% |
| Line | 4.435 ± 0.315 | 32 hr | 100% |

Table 2: **Average area and wound closure times for different wound shapes (N=3).**

# Discussion

The automated wound healing assay demonstrates notable advantages in terms of reproducibility, scalability, and experimental flexibility compared to traditional methods. The robotic control of the assay not only minimizes human variability but also ensures consistent wound creation and monitoring. The scalability and flexibility of our approach allows for high-throughput experimentation, making it adaptable to various experimental conditions and wound types. The incorporation of live-cell fluorescence microscopy in our automated workflow opens up avenues for assessing additional biological processes during wound healing. This real-time imaging capability enables the observation of dynamic cellular events, such as cell cycle phase transitions [12] or epithelial-to-mesenchymal transition (EMT) dynamics [13], providing a more comprehensive view of cellular behaviors in response to injury.

An exciting prospect of our automated workflow is its applicability to cellular reprogramming studies geared towards accelerating the wound healing process. In previous work, we have successfully reprogrammed human fibroblasts to embryonic stem cells, muscle cells, and other cell types utilizing our in-house data-guided control algorithm [7]. This framework employs a multi-way dynamical systems approach to predict combinations of TFs, as well as the specific time point in which TF activation or supression will have the greatest effect, for converting one cell type into another desired phenotype. We envision that by leveraging the precision and control offered by the AWH assay, future iterations of our model can be refined to explore the modulation of cellular states during wound healing through transcription factor-guided therapy, contributing to advancements in regenerative medicine.

Wound healing has long been recognized as a process akin to cancer metastasis [14, 15]. Keratinocytes have the innate ability to partially and reversibly transition into another phenotype. This feature of wound healing resembles that of the epithelial-mesenchymal transition (EMT), a process in which an epithelial cell acquires a mesenchymal phenotype. In cancer, EMT is known to be a key player in tumor progression, metastasis, and chemo-therapeutic resistance [16, 17]. In wound healing, this partial EMT is crucial to the restoration of epidermal barrier function. Keratinocyte cells proximal to the injury site lose

their epithelial characteristics and adopt a motile mesenchymal-like program, while cells distal to the wound edge begin to proliferate. As the underlying tissue repairs, keratinocytes repopulate the wound bed and reestablish their epidermal signature [15, 18].

Although it is known that chromosomal aberrations and certain core EMT genes are not apparent in physiological re-epithelialization [15], the evident similarities between cancer and wound healing mechanisms prompts the notion that deepening our understanding of the intricate balance between migration and proliferation during wound healing could augment our abilities to understand cancer metastasis. Human-relevant in vitro models have recently been approved by the FDA as a viable alternative to animal testing in preclinical drug evaluations [19]. Recognizing the well-documented pharmacogenomic variations between animal models and humans, the use of biomimetic cell-based assays for drug safety and efficacy testing represents a significant step toward more accurate predictions of human therapeutic responses. In the context of wound healing and cancer, our automated method can be harnessed to screen for potential EMT regulators and, in the long term, to evaluate the efficacy of anti-cancer drugs targeting this process.

# Conclusion

We have developed an automated workflow for the execution and analysis of in vitro wound healing experiments. Our automated wound healing assay not only addresses the limitations of traditional methods but also opens up avenues for exploring diverse biological phenomena during wound healing and advancing research in regenerative medicine and cancer biology. The reproducibility, scalability, and adaptability of our approach, coupled with its potential applications, position it as as valuable tool in the broader landscape of experimental techniques.

# Acknowledgments

This work is supported by the Air Force Office of Scientific Research under award number FA9550-22-1-0215, Defense University Research Instrumentation Program (DURIP) 2018, DURIP 2022, and MATHWORKS.

# Methods

## Automated wound healing assay

Any multi-well plate with 6 to 96 wells can be used for the AWH assay. The following **Plate calibration** steps need to be completed once for each plate size used. We recommend measuring the **Tip to stage offset** for each new dispensing tip used with the calibrated well plate.

### Plate calibration:

1. Place the desired well plate onto the BAB Print Stage and de-lid the plate.
2. In the BAB HMI, navigate to the **Control** tab, select **Other**, and retrieve the BAB Printing Tool.

3. In the **Containers** tab, select **Plates**, and create a new container for printing. Enter the number of rows and columns for the well plate.

4. Manually position the tip on the end of the Printing Tool in the center of the first well (A1). *The tip does not need to be touching the bottom surface of the well as the z coordinate will be automatically updated in the following steps.*

5. Select **Get Current** under the **First Well Pipette Location** prompt to store the x, y, and z coordinates of A1.

6. Repeat steps 4-5 for the **First Row, Last Well Pipette Location** and **Last Well Pipette Location**.

7. Save the stored positions, select **Printing Calibration**, and select **Measure Tip**.

8. Repeat steps 4-5 for all four corner wells of the plate.

9. Select **Update** under **Update All Wells (Relative)**, and select **Calculate** under **Calculate Wells from Extents** to store the positions for all wells in the plate.

**Tip to stage offset:**

1. Select the desired tip size and place the tip on the end of the BAB Printing Tool.

2. Navigate to the **Calibration** tab and select **Offset**.

3. Manually position the tip so that it is touching the bottom surface of a well in the plate. *The tip should not be pressing into the plate surface to the point where the tip is deforming.*

4. Select **Measure Tip Offset** and save the results.

**Wound design:**

1. Create a new file in the Tissue Structure and Information Modelling (TSIM) application.

2. Under the **project settings** tab, select the multi-well plate size that will be used when running the assay to provide a reference template in TSIM. Ensure the **print continuously** box is checked and the **move between layers** is set to printer default.

3. Select **create a sketch** and choose a plane parallel to the well plate template.

4. Using the sketching tools available in TSIM, draw the desired wounds in the respective wells. *Different wound shapes can be drawn in the same plate. Each wound shape needs to be sketched once, as the final "wounds" can be copy and pasted into the other wells.*

5. Select **create a tube along a sketched surface**, and select the sketched wounds. Check the **flatten** box.

6. Under the **objects** tab, set the z-coordinate of all objects to 0.0001 to flatten the wounds onto the plate surface.

7. Navigate to the **materials** tab, and set the **pressure** to 0 psi. Adjust the printing acceleration and speed as needed.

8. Under the **print jobs** tab, select the file and **send print job** to the BAB HMI.

**Execution of AWH assay:**

1. Ensure that no tool is present on the BAB Arm.

2. Navigate to **Calibration**, select **Offset**, and **Load** the saved tip offset from the previous steps.

3. Navigate to the **Print** tab and select the designed wound file under **Print Job**.

4. Choose the calibrated well plate as the container for printing under **Select Calibrated Well Plate**, and select **Start**.

5. Select the storage bay containing the BAB Printing Tool.

6. Press **GO**.

## Cell culture

Human BJ fibroblasts (ATCC CRL-2522) were cultured on standard cultureware in Dulbecco's Modified Eagle's Medium (DMEM, Gibco 11965-092) with 10% Fetal Bovine Serum (FBS, Corning 35-015-CV), 1% MEM Non-Essential Amino Acids (NEAA, Gibco 11140-050), and 1% penicillin-streptomycin (P/S, Gibco 15140122). Cells were incubated at 37°C in 5% $CO_2$, and media was exchanged every 48 hours. For the AWH assay, BJ Fibroblasts were seeded at densities ranging from 0.22 - 0.63 x $10^5$ cells/$cm^2$ in 12-, 24-, or 96-well plates. After 24 hours, cells were incubated in normal media containing 0.02 $\mu$M Hoechst 33342 (Enzo, ENZ-52401) for 2 hours, followed by executing the AWH assay. Wells were then washed twice with PBS. FluoroBrite DMEM (Gibco, A18967-01) with 10% FBS, 1% NEAA, and 1% P/S was added to all wells prior to image acquisition.

## Image acquisition

The Ziess Celldiscoverer 7 (CD7) live-cell imaging system was used to automate the acquisition of time-lapse images over the course of wound closure. Oblique contrast and fluorescence microscopy was performed using the CD7 microscope with a Plan-Apochromat 5x/0.35 objective and 1x tube lens. Images were captured using an Axiocam 506 with 14 bit resolution. Two LED modules (385 nm and 725 nm) were used simultaneously. The following filter sets were used for fluorescence microscopy: H3342–348 nm; 414, 529, 673 nm; 458-474, 546-564, 618-756 nm (excitation; beam splitter; emission filter). Cells were imaged at 37°C in 5% $CO_2$. Images were captured every 30 minutes over the duration of wound closure. For each wound, a multi-channel time-series `ome.tiff` file was prepared in the Zen Blue 3.0 software and exported for downstream analysis.

## Image processing

To automate analysis of wound healing experiments, we constructed an image processing pipeline using the `Python` framework `Snakemake` [20, 21]. The pipeline is designed to manage parallel processing of large time-series imaging data in a high-performance computing environment. Briefly, the pipeline produces nuclear segmentations at each timestep using `StarDist` [22] and predicts cellular movement using a Bayesian single cell tracking approach [23]. Inputs to the pipeline are multi-channel time-series `ome.tiff` files and a set of user-defined parameters controlling the behavior of different filtering and analysis operations [24]. The outputs of the pipeline are properties of cell nuclei at each time step, and nuclear linkages between time-steps which we refer to as 'tracks.'

We describe the operations of the pipeline in Algorithm 1 on a single input. Note that the pipeline may be run on a set of input images.

**Algorithm 1** Automated Cell Tracking

**Input:** Image $\mathbf{H}_{(c \times t \times y \times x \times q)}$ where $c$ is the number of color channels, $t$ is the number of timesteps in the `ome.tiff` file, $y$ is the number of vertical pixels, $x$ is the number of horizontal pixels, and $q$ is the RGB index.

**Output:** Track table $\mathbf{X}_{(r \times m)}$ where $r$ is the number of segmented nuclei times the number of timepoints in their respective tracks and $m$ is the number of features for analysis, e.g., estimates of nuclear size, shape, and fluorescent intensity over each color channel.

1: **Flatten:** The RGB channels of image $\mathbf{H}$ are converted to greyscale resulting in a new image shape $\bar{\mathbf{H}}_{(c \times t \times y \times x)}$

2: **Rescale dimensions:** Image $\bar{\mathbf{H}}$ is rescaled over spatial dimensions $y, x$ according to user-defined parameters.

3: **Rescale intensities:** Image $\bar{\mathbf{H}}$ is rescaled over color channels $c$ to [0, 255]

4: **Median filtering:** A median filter is applied to $\bar{\mathbf{H}}$ based on user-defined parameters.

5: **Histogram equalization:** Adaptive histogram equalization is applied to $\bar{\mathbf{H}}$ based on user-defined parameters.

6: **Segment:** Image $\bar{\mathbf{H}}$ is segmented using `StarDist` on the nuclear channel [22]. Segmentation results are stored as a properties table using `skimage.region_props()` [24].

7: **Track:** Segmentation results are linked over time using `btrack` [23]. The resulting table is merged with the nuclear properties table and stored as $X$.

# References


[1] Gregory S. Schultz et al. "Principles of Wound Healing". In: *Mechanisms of Vascular Disease: A Reference Book for Vascular Specialists*. Ed. by Robert Fitridge and Matthew Thompson. Adelaide (AU): University of Adelaide Press, 2011. ISBN: 978-0-9871718-2-5.

[2] Rafik Boudra and Matthew R. Ramsey. "Understanding Transcriptional Networks Regulating Initiation of Cutaneous Wound Healing". In: *Yale J Biol Med* 93.1 (27, 2020).

[3] Matthias Schäfer and Sabine Werner. "Transcriptional Control of Wound Repair". In: *Annual Review of Cell and Developmental Biology* 23.1 (2007).

[4] Elisabeth Hofmann et al. "Human In Vitro Skin Models for Wound Healing and Wound Healing Disorders". In: *Biomedicines* 11.4 (2023).

[5] Nafise Amiri et al. "Roles of cutaneous cell-cell communication in wound healing outcome: An emphasis on keratinocyte-fibroblast crosstalk". In: *Experimental Dermatology* 31.4 (2022).

[6] Meirong Li et al. "Epithelial-mesenchymal transition: An emerging target in tissue fibrosis". In: *Exp Biol Med (Maywood)* 241.1 (2016).

[7] Scott Ronquist et al. "Algorithm for cellular reprogramming". In: *Proceedings of the National Academy of Sciences* 114.45 (7, 2017).

[8] Reza Riahi et al. "Advances in Wound-Healing Assays for Probing Collective Cell Migration". In: *SLAS Technology* 17.1 (1, 2012).

[9] Sixun Chen et al. "An effective device to enable consistent scratches for in vitro scratch assays". In: *BMC Biotechnology* 23.1 (28, 2023).

[10] Wendy Gough et al. "A Quantitative, Facile, and High-Throughput Image-Based Cell Migration Method Is a Robust Alternative to the Scratch Assay". In: *SLAS Discovery* 16.2 (1, 2011).

[11] Deyber Arley Vargas Medina, Edvaldo Vasconcelos Soares Maciel, and Fernando Mauro Lanças. "Modern automated sample preparation for the determination of organic compounds: A review on robotic and on-flow systems". In: *TrAC Trends in Analytical Chemistry* 166 (1, 2023).

[12] Amar M. Singh et al. "Utilizing FUCCI reporters to understand pluripotent stem cell biology". In: *Methods (San Diego, Calif.)* 101 (5, 2016).

[13] Meredith S. Brown, Kristen E. Muller, and Diwakar R. Pattabiraman. "Quantifying the Epithelial-to-Mesenchymal Transition (EMT) from Bench to Bedside". In: *Cancers* 14.5 (2022).

[14] Howard Y. Chang et al. "Gene Expression Signature of Fibroblast Serum Response Predicts Human Cancer Progression: Similarities between Tumors and Wounds". In: *PLOS Biology* 2.2 (13, 2004).

[15] Daniel Haensel and Xing Dai. "Epithelial-to-mesenchymal transition in cutaneous wound healing: Where we are and where we are heading". In: *Developmental Dynamics* 247.3 (2018).

[16] Douglas Hanahan and Robert A. Weinberg. "Hallmarks of Cancer: The Next Generation". In: *Cell* 144.5 (4, 2011).

[17] Anushka Dongre and Robert A. Weinberg. "New insights into the mechanisms of epithelial–mesenchymal transition and implications for cancer". In: *Nat Rev Mol Cell Biol* 20.2 (2019).

[18] Adriana Zanca, Jennifer A. Flegg, and James M. Osborne. "Push or Pull? Cell Proliferation and Migration During Wound Healing". In: *Frontiers in Systems Biology* 2 (2022).

[19] Peter-James H. Zushin, Souhrid Mukherjee, and Joseph C. Wu. "FDA Modernization Act 2.0: transitioning beyond animal models with human cells, organoids, and AI/ML-based approaches". In: *J Clin Invest* 133.21 (1, 2023).

[20] Johannes Köster and Sven Rahmann. "Snakemake—a scalable bioinformatics workflow engine". In: *Bioinformatics* 28.19 (2012).

[21] Felix Mölder et al. "Sustainable data analysis with Snakemake". In: *F1000Research* 10 (2021).

[22] Martin Weigert et al. "Star-convex Polyhedra for 3D Object Detection and Segmentation in Microscopy". In: *2020 IEEE Winter Conference on Applications of Computer Vision (WACV)*. Snowmass Village, CO, USA: IEEE, 2020. ISBN: 978-1-72816-553-0.

[23] Kristina Ulicna et al. "Automated Deep Lineage Tree Analysis Using a Bayesian Single Cell Tracking Approach". In: *Frontiers in Computer Science* 3 (2021).

[24] Stéfan van der Walt et al. "scikit-image: image processing in Python". In: *PeerJ* 2 (2014).